Research Article Vol. 59, No. 21 / 20 July 2020 / Applied Optics F1

applied optics

Subsuns and rainbows during solar eclipses

GUNTHER P. KÖNNEN,[1,*] GLENN SCHNEIDER,[2] EVAN H. ZUCKER,[3] AND PANU LAHTINEN[4]

[1]Royal Netherlands Meteorological Institute (KNMI), The Netherlands (retired)
[2]Steward Observatory and Dept of Astronomy, The University of Arizona, Tucson, Arizona 85721, USA
[3]Totality Software, Inc., San Diego, California 92131, USA
[4]Finnish Meteorological Institute, Finland
*Corresponding author: konnen@planet.nl

Received 9 January 2020; revised 14 April 2020; accepted 19 April 2020; posted 20 April 2020 (Doc. ID 387716); published 29 May 2020

A photographic observation sequence was obtained of a subsun before, during, and after the total phase of the 2016 solar eclipse. The time-resolved images were obtained from a high-altitude jet aircraft. The image sequence was searched for the possible presence of a solar corona-generated subsun during totality. Although the subsun-creating conditions apparently persisted during totality, the drop in signal intensity compared to the local background prevented its detection. Separately, we document a visual observation from the 1977 total solar eclipse of a rainbow that faded, in the last a few seconds before totality, from being normally multicolored to monochromatic red from water drops then predominantly illuminated by light from the solar chromosphere. A similar transition in the final seconds before, and after, totality is expected to occur for parhelia. The posited short-living monochromatic red parhelion resulting from the momentary illumination of ice crystals by the solar chromosphere is still waiting to be observed.

https://doi.org/10.1364/AO.387716

1. INTRODUCTION

During the progress of the partial phase of a solar eclipse, the partially eclipsed solar disk—or, more precisely, the partially eclipsed solar photosphere—remains for the majority of time the dominant light source. This means that the signal-to-background ratio of atmospheric-optical phenomena like rainbows or halos remains the same. So, although during the progress of the partiality the overall light level of the environment decreases, the contrast and, thus, visibility of such atmospheric phenomena remain essentially constant. This situation changes during the last ∼30 s before totality, when the solar photosphere loses its role as the primary light source and its role is overtaken by the ∼10^6 times fainter solar corona. However, during totality, the intensity of skylight has decreased by merely a factor 10^3-10^4 compared with the normal day value [1–4], with ∼4000 as the typical central value [1]. A previous study [1] indicated that certain intrinsically bright halos may survive the accompanying drop of a factor 250 in signal-to-background ratio, and that rainbows formed from the light of the solar corona are most likely doomed to disappear in the residual brightness of the eclipse sky.

Among the brightest halos are those caused by refraction of (Sun)light by two faces of hexagonal ice crystals forming a prism with wedge angle 60°. If the crystals are randomly oriented, this results in a colored circular halo with a radius 22° and centered at the light source [5–7]. This so-called 22° circular halo is well known by the general public. However, falling ice crystals are subject to aerodynamic forces, which may cause some crystals, depending on their shape, to assume a certain preferential orientation in the sky. The transition from random to preferential orientation causes the 22° circular halo to break up in a variety of noncircular halos shaped as arcs or spots. These structures are positioned near the circular halo to which they are associated [5–7], the most prominent of them being the parhelia ("mock suns"), which are situated on either side of the Sun and the upper and lower tangent arcs to the 22° circular halo.

Parhelia and the tangent arcs are less well known but are intrinsically much brighter than the 22° circular halo to which they are associated [8] and, therefore, belong to the best candidates among the refraction halos to remain visible during totality. A halo phenomenon of intrinsic brightness that even may surpass that of a parhelion is the so-called subsun [5–7], which belongs to the class of reflection halos and arises from reflections of light in a swarm of preferentially oriented ice crystals having at least one face horizontal. However, this halo appears below the horizon and is therefore only visible for observers who happen to be situated higher than the subsun-generating crystals (see Fig. 1).

In most cases, the crystals that create the subsun are shaped as thin hexagonal plates, like the one depicted in Fig. 1. There are three different subsun-making light paths via this kind of crystal. For two of them, the reflection takes place at the (horizontally oriented) lower basal face of the crystal; for the third and simplest subsun-making path, the reflection takes place at the (horizontally oriented) upper basal face of the crystal

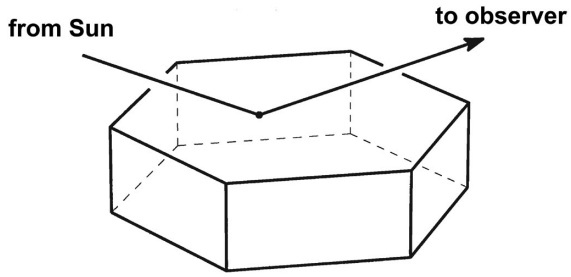

Fig. 1. A subsun arises from preferential oriented ice crystals with at least one of its faces horizontally oriented. In most cases, the subsun-generating crystals are hexagonal plates, oriented as depicted in this diagram. External reflection of Sun light at the horizontally oriented upper face creates a subsun.

and consists of a simple external reflection (see [5]). The direction of the outgoing ray for all three paths is the same, being the same as in the case of reflection off a horizontal (water) surface.

The ensemble of horizontally oriented crystal faces in the air mass below the observer acts as a giant three-dimensional mirror, in which the mirror image of celestial objects like the Sun or the Moon [9], or even Jupiter, [10] may appear.

The subsun is frequently seen by air passengers seated on the Sun-side of an airplane. When the subsun occurs, it appears at the so-called subsun point—the point on the celestial sphere whose azimuth is the same as that of the Sun, and whose elevation is minus that of the Sun with respect to the true horizon. This is the same point where the sunglint [11]—the mirror image of the Sun in a still lake—appears. The difference between a reflection by a water surface and a reflection by a three-dimensional set of horizontal reflecting crystal faces is that the latter is incapable of producing a mirror image of a nearby object, for instance, of a passing aircraft.

Usually, the subsun is somewhat elongated [5–7] instead of being perfectly round—just like the Sun's mirror image in rippled water [11]. This happens because the horizontal alignment of the subsun-generating crystal faces is usually not absolutely perfect. If the subsun-generated crystals are in a layer of the atmosphere with much turbulence, like near the tops of cumulus clouds, then the subsun assumes an irregular and temporally variable shape [12].

Observing a subsun created by the light of the solar corona requires the observer to be positioned higher than the halo-generating ice crystals during a total solar eclipse—a condition which will be rarely fulfilled by chance. However, during the March 2016 total solar eclipse, a deliberately [13] 25-min-delayed Alaska Airline Anchorage–Honolulu flight intercepted the lunar umbra, and the totally eclipsed Sun was seen from the plane, as planned in detail by one of us (G. S.; see [13]). One of us (E. Z.), on board the plane, obtained a constant-cadence time series of wide-angle pictures flanking and during the 1 m 52 s of totality seen. The pre- and post-totality images of that series show a subsun. It seems plausible that the conditions causing the subsun persisted during totality itself. This provides a first opportunity to empirically check the apparent (non)persistence of a subsun during totality.

In the previous study about the visibility of atmospheric-optical phenomena during eclipses [1], it was concluded that rainbows, unlike halos or diffraction coronas, are very unlikely to remain visible during the totality stage of a solar eclipse. So far, no counterexample to this conclusion is reported, but it appears that a rainbow can undergo a spectacular transformation just before it disappears and/or reappears after third contact (end of totality). We document a visual observation, taken just seconds prior to the totality phase of the October 1977 solar eclipse, of a monochromatic red rainbow resulting from the illumination of raindrops by the solar chromosphere at the stage when the photosphere was already completely covered by the lunar disk.

The organization of the current paper is as follows. First, we analyze and discuss the appearance of the subsun near and during the total phase of the 2016 solar eclipse in order to refine the previous conclusions [1] about the visibility of halos during total solar eclipses. Second, we describe and discuss the appearance of a monochromatic red rainbow just prior to the totality of the 1977 solar eclipse and discuss which halos may undergo a similar multispectral-to-monochromatic-red transformation in the very last seconds before totality.

By absence of an established nomenclature for rainbows and halos generated by light sources other than the Sun or Moon, we adopt in this paper a system in which the nature of the primary light source is indicated by a prefix: in our case "coronal" or "chromospheric." So, if the primary light source is the solar corona, then scattering by raindrops may result in a coronal rainbow, and scattering by ice crystals in coronal halos, a coronal subsun, or coronal parhelia. Similarly, if the primary light source is the solar chromosphere, then we may have a chromospheric rainbow, chromospheric halos, a chromospheric subsun, or chromospheric parhelia. However, if the primary light source is the solar photosphere, then no prefix is added, which is consistent with common terminology [5].

2. SUBSUN DURING THE SOLAR ECLIPSE OF 9 MARCH 2016 (UTC)

A. Subsun Observation

The observation of the eclipse-related subsun took place during a commercial daytime flight from Anchorage (61.17° N, 150.00° W) to Honolulu (21.33° N, 157.92° W), operated by Alaska Airlines. The Boeing 737-800 of flight AS870 originating on 8 March 2016, took off at 23:15 UTC.

The aircraft heading was basically south, with a deviation to its usual track on the approach to, and through, the lunar umbral shadow. As planned [13], the aircraft at flight level (FL) 350 (corresponding to 35,000 feet = 10.7 km above mean sea level) and groundspeed of 447 kts (828 km/h or 0.23 km/s) crossed nearly perpendicular to the centerline-track of the 107 km wide umbral shadow at 03:36:00 (±2 s) UTC at 31.30° N, 156.18° W. At that location, the magnitude of the eclipse was 1.0155. The lunar shadow that had approached and overtaken the aircraft from azimuth 261° was traveling at 5.16 km/s (18,600 km/h) at mid-eclipse. During the 112 s of totality, the Sun altitude angle above the true horizon went from 10.5° to 10.1°, and its azimuth went from 258.2° to 258.6° while the aircraft covered a distance of 26 km. The aircraft's true heading of 168.5° offered the passengers seated on the right side

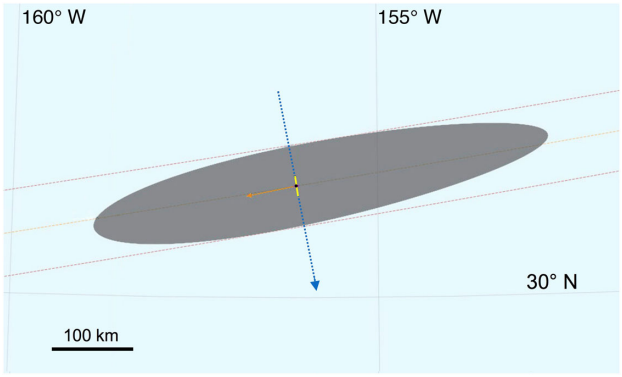

Fig. 2. Blue stippled line: path of the aircraft during the last 9 min before and the 9 min after the instant of its mid-eclipse intercept (MEI, on 03:36:00 UTC). Yellow solid line: aircraft's path during totality. The gray area is, for 03:36:00 UTC, the projection of the Moon's umbral shadow onto the Earth (at elevation 10.7 km above mean sea level). The upper, lower, and middle parallel dashed lines, respectively, represent the path of totality's N, S limits, and centerline. The lunar umbra moves along this path from W (left) to E (right) with a speed of 5.2 km/s. The orange arrow at the MEI-position shows the direction toward the Sun, which is in the direction in which the Moon's shadow approached the aircraft.

of the plane an optimal view to the eclipse: in that geometry, the umbral shadow approached and enveloped the subsun point and (later) the aircraft from the horizon essentially along the direction of the line of site to the Sun as seen "straight out" the Sun-side aircraft windows. Figure 2 depicts the path of the aircraft for 9 minutes before and after its mid-eclipse intercept and the position of the Moon's umbral shadow at the instant of the aircraft's mid-eclipse intercept.

The photographic observation started 11 min before totality. Until 4 min before totality, five test pictures plus one test burst consisting of three frames were taken. These six initial observations, taken at irregular intervals, covered the 7 min test phase with a time resolution of ∼1−2 min. The camera used was a Sony SLT-A77V Camera. It was mounted on the aircraft window and could be operated automatically. The actual eclipse run started 3 min later: from 1 min before totality until 1 min after totality, 135 pictures were taken with fixed intervals of 2 s. Exposure time (1/90 s), aperture ($f/4.0$), and ISO (400) remained fixed throughout the observation. The focal length of 11 mm (corresponding to 16 mm for 35 mm frames) corresponds to horizontal and vertical fields of view of the pictures of 115° and 75°, respectively. The uncertainty of the absolute UTC calibration for each image frame was ±2 s; a relative uncertainty of about ±1.5 s is estimated for the duration of totality (difference in UTC between C3 and C2) as determined from the images acquired with an interframe cadence of 2 s.

The pretotality pictures clearly show a bright subsun straight under the Sun, superimposed upon the cloud tops (Fig. 3, top). This subsun disappeared 14 s before totality as seen from the aircraft. 12 s before totality ended, light at the subsun spot reappeared (Fig. 3, bottom). 6 s later, thus 6 s before the end of totality as seen from the aircraft, there is an increase in the size of the lighting area at the subsun spot, resulting in an extra gain in its total intensity. Table 1 gives the times of the key moments of the observation.

Fig. 3. Top: pretotality. The white spot straight under the Sun is the subsun. The dark patch on the clouds under the Sun is the rapidly approaching lunar umbra. The green spot is an artifact due to internal reflections in the camera lens (frame ID #3668, taken 28 s before totality). Bottom: During the final moments of totality, the subsun reappeared superimposed upon the clouds below that are already directly lit by the solar photospheric light (frame ID #3734, taken 2 s before totality ended). Pictures taken by Evan Zucker, 9 March 2016 (UTC); horizontal field of view is 115°. A video showing the time-lapse sequence of the images recorded before, during, and after totality [3 frames/second, date/time according to Hawaiian Standard Time (UTC-10)] can be viewed in Visualization 1.

B. Meteorological Conditions

The ERA5 [ERA stands for European Centre for Medium-Range Weather Forecasts (ECMWF) re-analysis] dataset provides temperature, specific humidity, and wind at an hourly time resolution on a worldwide grid of 31 km spatial resolution, for 137 atmospheric layers between 10 m and 80 km above ground level [14]. This new reanalysis project is currently in progress by the ECMWF and aims to cover the period 1950 until present. Sea surface temperatures are provided also. At the moment of writing, the data from year 2000 onward are already available. The temperature and humidity data of 03:00 and 04:00 UTC of 9 March 2016, were downloaded and interpolated by layer to the aircraft's position at mid-eclipse (31.3° N, 156.2° W). Figure 4 shows the 03:00 UTC vertical temperature (T) and dew point (T_d) vertical profiles; Table 2 shows the main characteristics of the 03:00 and 04:00 UTC profiles.

Table 1. Timeline of Zucker's Observation (Flight AS 870, Anchorage–Honolulu)

Frame ID #	Event	UTC	Time from C2
–	take off (8 March)	23:15:54	–
3645–3652	8 test pictures taken	03:24–03:31	−11 min until −4 min
3653	start photo sequence	03:33:56	−1 min 6 s
3676	subsun disappears in umbra	03:34:48	−14 s
3682–3683	start totality (C2)	03:35:02	0 s
3709–3710	mid totality	03:36:00	+58 s
3729	light returns at subsun point	03:36:42	+1 min 40 s
3732	light at subsun point gains extra intensity	03:36:48	+1 min 46 s
3735	end totality (C3)	03:36:54	+1 min 52 s
3787	last picture taken	03:39:46	+3 min 44 s
–	landing	05:34:31	–

The most prominent tropospheric feature in the vertical profiles is the subtropical subsidence inversion at a height of 5 km, which forms the border between very dry (dew point depression $T - T_d > 25°C$) air higher up, and moist air ($T - T_d < 3°C$) below it, the latter air mass extending down to ground level. A second inversion layer is present at ∼600 m, being a (weak) boundary layer inversion. The sea surface temperature is considerably (by 5°C) higher than the 10 m air temperature. This is caused by the presence of a highly superadiabatic atmospheric surface layer (thickness typically of order 50 m)—triggering atmospheric instability higher up and feeding convective activity with formation of cumuliform clouds. The presence of the two inversion layers indicates cloud formation in two atmospheric levels, which is in accordance with the photographic pre- and post-totality observations (see Section 2.C). According to the temperature profile, the lower clouds have their tops at the boundary layer inversion (∼600 m); the higher clouds have their tops at subtropical inversion layer (∼5 km), where the temperatures are amply below freezing. The aircraft flew in a dry air mass (at 10.7 km), thus amply above the atmospheric levels where cloud formation could occur. A comparison of the 03:00 and 0:400 UTC profiles shows that the top of the subtropical inversion layer sank in this time span by 300 m and its width increased from 300 m to 1100 m, meaning that the inversion was losing its sharpness. This development is indicative for a decrease in convective activity during the hour that deep-eclipse occurred.

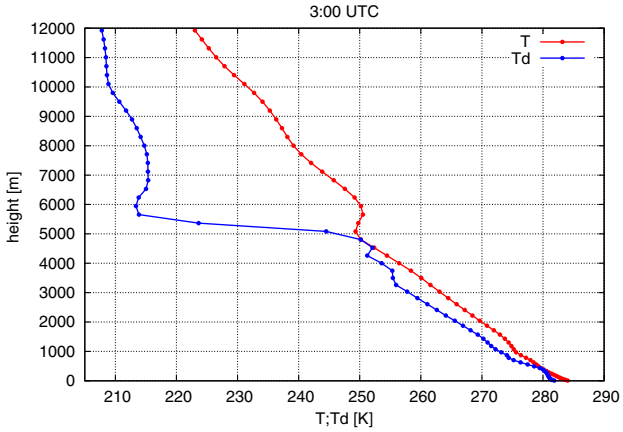

Fig. 4. Temperature (T) and dew point (T_d) vertical profiles of 9 March 2016, 03:00 UTC, at the mid-eclipse position (retrieved from ERA5 reanalysis run; Kelvin temperature scale).

C. Subsun Identification

The test pictures show that, prior to totality, the ocean was partly cloudy, being covered with clusters made up from small low-level cumulus clouds. In big gaps between the clusters, a broad sunglint from the ocean surface was seen. About 2 minutes prior to totality, the aircraft flew into a region where a higher altitude cloud layer completely obscured the lower one.

In all pretotality pictures, the subsun point lights up (see Fig. 3, top) until being extinguished by the lunar umbra, 14 seconds before C2 (Table 1). There is little doubt that the feature is indeed the subsun, as it exhibits the typical shape of a subsun

Table 2. Specific Points in the Vertical Temperature Profiles at the Mid-Eclipse Position

	03:00 UTC		0:400 UTC	
	Height	Temperature	Height	Temperature
Sea surface	0 m	+16.0°C	0 m	+16.0°C
Lowest ERA5 level	10 m	+10.9°C	10 m	+11.4°C
Boundary layer inversion	600 m	+5.3°C	700 m	+5.1°C
Freezing level	1540 m	0°C	1450 m	0°C
Subtropical inversion, bottom	5100 m	−23.8°C	4000 m	−17.0°C
Subtropical inversion, top	5400 m	−23.4°C	5100 m	−21.4°C
Aircraft's flight level	10700 m	−45.2°C	10700 m	−45.2°C
Tropopause	16300 m	−65.0°C	16300 m	−63.7°C

generated in crystal layers over cumuliform clouds [12] and the cloud layer seems unbroken.

After the lunar umbra had passed the subsun point, its light returned. This happened at frame ID #3729, 12 s before frame ID #3735, where, as seen from the aircraft, totality had ended. Figure 5 shows, in 11 frames, the return of light in the subsun point and of the light of the photosphere of the Sun.

The time difference between the return of light at the subsun and at the aircraft is caused by the fact that the incidence angle of the lunar shadow is inclined to the Earth surface. This inclination results in a dependency of second and third contacts (C2 and C3) on the altitude of the observer (aircraft) above mean sea level. By flight plan design [13,15], the azimuth of the Sun and the azimuth from which the lunar umbra approached the site were nearly (within 3°) the same, and perpendicular to the path of the aircraft (see Fig. 2). Then, it follows from simple geometry that the difference Δz between the height of the aircraft above mean sea level and the maximum possible height of the reflecting surfaces in the subsun point to be lit by the solar photosphere is given by the following two equations:

$$\cos(2\delta + h) = \cos(h) - \frac{v\Delta t}{R_{\text{aircraft}}}, \quad \textbf{(1)}$$

$$\Delta z \equiv R_{\text{aircraft}} - R_{\text{crystal}} = R_{\text{aircraft}}\left[1 - \frac{\cos(2\delta + h)}{\cos(\delta + h)}\right], \quad \textbf{(2)}$$

where h is the Sun altitude angle above the true horizon (which is at flight altitude 10.7 km $\sim 3.2°$ above the apparent horizon—see Fig. 5), Δt is the time lag between the reappearance of light in the subsun point, and v is the velocity of the lunar umbra on the terminator plane—which is the plane through the Earth's center whose normal points to the center of the Sun—*minus* the velocity of the observer's position due to the Earth's rotation, also projected onto that plane. In our case, $v = 1.00 - 0.08$ km/s $= 0.92$ km/s. R_{aircraft} and R_{crystal} are the distances to the Earth's center of the aircraft and of the reflecting crystal, respectively. Furthermore, δ is the great-circle distance between the observer and the Sun-reflecting surface. Figure 6 depicts the geometry of the problem; Table 3 shows for $h = 10°$ the results for δ and Δz.

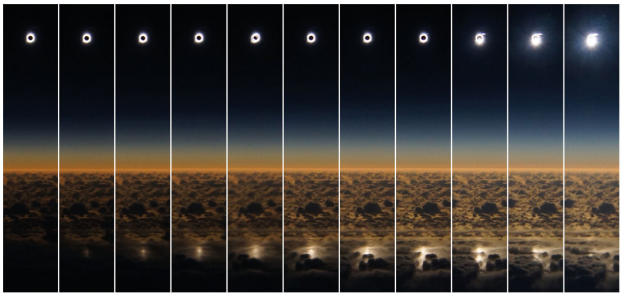

Fig. 5. Shortly before the end of totality, the light returns at the subsun point. Third contact (C3) occurs at the eighth frame of this composite consisting of 11 frames. The individual frames are mutually separated by 2 s; the 20 s sequence runs from C3–14 s until C3 + 6 s (frame ID #s 3728–3738). At this aircraft height (10.7 km), the horizon is depressed by ~3.2° and is thus angularly closer to the subsun point than to the Sun. With the Sun 10.1° above the true horizon at C3, the line-of-site distance from the aircraft to the subsun point at sea level is ~62 km.

Table 3 leads us to the following conclusion: given the height of the aircraft (10.7 km), the first light at the subsun point happened when the lower boundary of the umbral conic had reached at the subsun point an atmospheric layer 5.7 ± 0.5 km below the aircraft as determined from these images (Table 3), thus a height of 5.0 ± 0.5 km above sea level. The temperature in that level (order −20°C; see Table 2) is well below freezing and allows for ice crystal formation; its height as deduced from Eqs. (1) and (2) (see Table 3) corresponds within the uncertainty to the height of the subtropical inversion layer as inferred from the vertical profile (Fig. 4 and Table 2). This makes the identification of the bright spot as being the subsun positive. The extra gain in subsun brightness at 6 s after its reappearance can be attributed to the rapidly increasing illumination of the subsun-making ice crystals by the photosphere just after C3, as the other mechanism—the presence of a second subsun-creating crystal layer 2.8 km below the aircraft (Table 3), thus ~ 8 km above sea level—is inconsistent with the observed low humidity at that atmospheric level (Fig. 4).

After its reappearance, the subsun kept the same irregular appearance as the pretotality subsun. The subsun persisted until frame ID #3762 (58 s after C3), when the subsun point approached the boundary of the upper cloud layer. From frame ID #3776 (88 s after C3) onward, the subsun point moved over a region of broken clouds with large areas of clear sky, and the subsun was replaced by a sunglint.

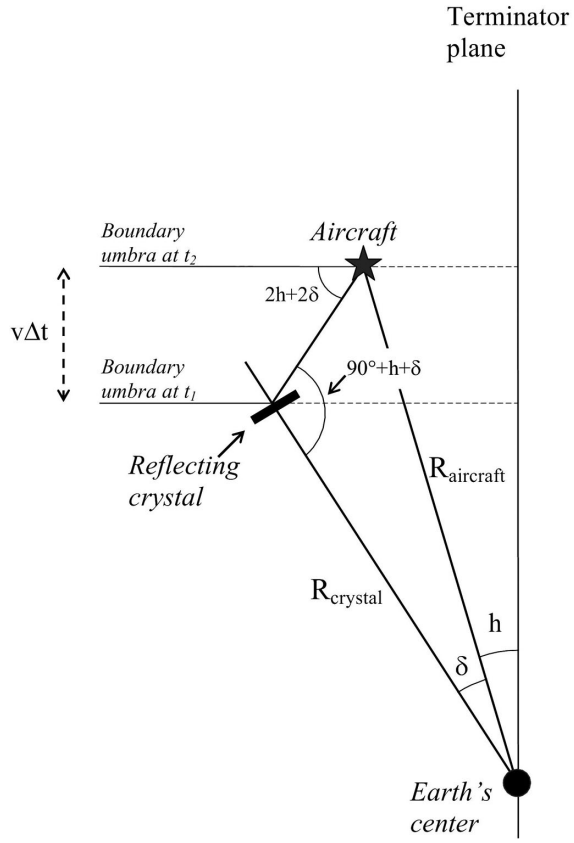

Fig. 6. Geometry of the reappearance of the subsun, shortly before the end of totality as seen from the aircraft [Eqs. (1) and (2)]. The Sun's altitude as seen from the aircraft is h; the Sun's altitude as seen from the reflecting crystal is $h + \delta$.

Table 3. Depth below the Aircraft of the Features at the Subsun Point Seen in Fig. 5

Frame ID #	Time	δ	Δz (km)[a]	Event
3729	C3–12 s	$0.27 \pm 0.02°$	5.7 ± 0.5	first light appears
3732	C3–6 s	$0.14 \pm 0.02°$	2.8 ± 0.5	extra brightness

[a]The error bars stem from the uncertainty in the exact timing of these two events.

Our analysis indicates that during pre- and post-totality, the line of sight to the ocean happened to be obscured by a temporary, almost unbroken cloud layer having their tops at the subtropical subsidence inversion—hence in a region where the atmospheric conditions are favorable for subsun formation. It is plausible that the same situation applied to the ∼2 min of totality.

D. Coronal Subsun?

A search for a photographic signal of the coronal subsun was undertaken with frame IDs #3680–3726. These 47 frames were all taken during the time span that both the aircraft and the subsun point were in the lunar umbra. The original raw CCD frames, separated into their RGB color channels by de-Bayering [16], were used as input for the numerical calculations, so the full dynamic range of the sensor data was available. The analog-to-digital conversion in the used camera in this image series was 12 bits. The series of images were coaligned and stacked to build a signal-to-noise ratio (SNR) using Halostack software [17]. The original raw images were used as input. A small area centered at the Sun is used as a reference for the image-correlation-based alignment. The images are translated with full-pixel offsets so that the locations of best correlation (R^2) match. The aligned images were saved individually as 16-bit PNG images to retain the maximum image quality, and different stacking methods (maximum, median, average) were tested. Out of the tested methods, the average of all the images gave the best start point for further image enhancements yielding a reduced image with lowest noise and cleanest subhorizon view by smoothing the clouds due to apparent movement.

The resulting image was contrast enhanced in image editing software (GIMP). To provide better details in the area of interest, first, the image dynamic range (minimum to maximum) was adjusted. As the image transfer function is inherently linear (doubling the scene brightness doubles the pixel value), applying a gamma correction (nonlinear mapping) makes some image details more readily visibly discernable. Further, an unsharp mask (USM) was applied to increase local contrast. None of these enhancements, however, brought out the coronal subsun with visual inspection.

3. CHROMOSPHERIC RAINBOW

A chromospheric rainbow was observed by one of us (G. S.) during an eclipse expedition to observe the the total solar eclipse of 12 October 1977, though totality itself was thwarted by clouds. The observing site was inland in Colombia, at 04° 51.8′ N, 74° 17.4′ W, on the side of the road #50 north of El Rosal, about 20 km NW of Bogota. The site was 10 km south of the central line of the 52 km wide eclipse path. The lunar umbra approached from west. The total phase of the eclipse occurred low to the horizon (9.2° elevation angle) in the west (azimuth 261.5°) with mid-eclipse at 22:03:30 UT, not long before sunset. The magnitude of the eclipse was 1.006; the totality lasted 49 s. G. S.'s personal account of the event (written up in 2017 in an email to G. K.) is based on his 1977-notes and his recollection:

"In the time leading up to totality, the sky was ∼80% completely clear, with low cloud only opposite in the sky toward the eastern horizon. It otherwise had been fully clear from the zenith westward. Soon prior to totality we could see a rainbow in the sky opposite the Sun toward where it was cloudy (presumably there was some rain there, but we could not see). In my recollection the rainbow consisted of an unbroken, more-or-less symmetrical arc (roughly equal length on both sides) with respect to the top. It did not extend fully to the horizon but nearly so. A very short time before totality a small, isolated, cumulous cloud formed from nowhere to the west of the zenith and began drifting toward the Sun. By complete bad luck it blocked the eclipse from our view for all 49 seconds of totality from where we were. However, the rainbow was illuminated prior to (and I would assume during) totality. Just prior to totality (in the final minute) the rainbow was uniformly fading from visibility, but in the last few seconds before (our clouded out) totality, the rainbow faded from view except for a bright single strand of hydrogen-alpha red. What we were seeing was obvious, but unexpected. The rainbow was for a few seconds only being illuminated by the solar chromosphere (only), and so we saw just a monochromatic arc! That was amazing but lasted only a couple of seconds at most. After the second contact, the rainbow disappeared in the eclipse-darkness. We got no pictures of the chromospheric rainbow, as all cameras were trained in the direction of the Sun, not opposite, hoping for a break in that one fatal cloud that never came until after totality!"

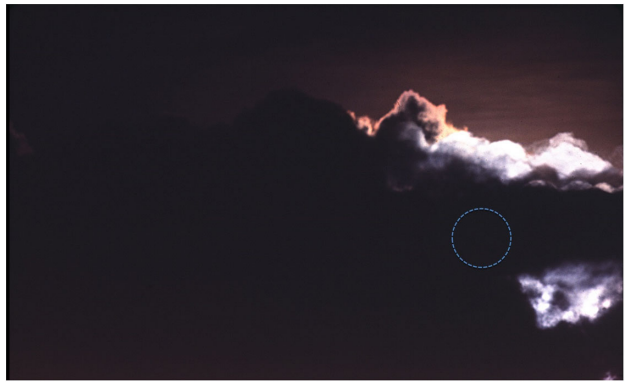

Fig. 7. Cloud that had covered the totally eclipsed Sun in October 1977. The picture is taken just after the end of the 49 s of totality. The deeply partially eclipsed Sun is behind a thick part of the cloud; the blue stippled circle marks the best estimate of the position of the solar disk. The white parts of the cloud edges are illuminated by the first rays of the solar photosphere. The red cloud edge is illuminated by nearly monochromatic red light from the chromosphere. A rainbow, at pretotality visible opposite in the sky, persisted during the last seconds before totality due to the light from the chromosphere while turning into a monochromatic red arc before it disappeared. The field size is 5.0° × 3.4°. (Picture taken by Glenn Schneider, rescanned from the original 35 mm slide.)

Figure 7 shows a picture of a part of the Sun-obscuring cloud opposite in the sky from the rainbow as taken through a 400 mm EFL lens, only seconds after third contact. The cloud is illuminated from behind. Its edge lights up because of near-forward scattering by cloud particles of the primary light source. The right part is white, as in the illumination, the light from the photosphere dominates. Behind it, there is a top of an apparently higher cloud element. Its edge is red, as the illumination comes predominately from the chromosphere—just as in the case of the transition from multispectral to monochromatic of the rainbow that happened shortly before the bow disappeared during totality.

4. DISCUSSION

A. Coronal Subsun?

The analysis of the sequence of 2016 eclipse pictures taken around totality strongly suggests that the subsun-creating conditions persisted during totality. Nonetheless, despite the brightness of the subsun in the pictures outside totality, a coronal subsun could not be seen in the pictures taken during totality—neither directly, nor after a significant contrast enhancement. A reason for this nondetection may be that the conditions for observing subhorizon halos during total solar eclipses from a high-flying platform may be less favorable than for above-horizon halos observed from the ground. The clouds against which subsuns usually appear are often thick and therefore bright compared to the background of cirrus, against which an above-horizon halo, like, for instance, bright parhelia, usually appear. This may reduce the signal-to-background ratio of coronal subsuns observed from aircraft below that of coronal parhelia observed from the ground, and possibly even down to the level that coronal subsuns become undetectable.

The current observation does not disprove the previous [1] claim that "Intrinsically bright halos seem to be capable to persist during totality." This refers in particular to parhelia and to the upper tangent arc to the 22° circular halo. Observing a coronal parhelion from the ground seems more likely than observing a coronal subsun from a high-flying plane.

A fascinating consequence of the observation of a chromospheric rainbow described in Section 3.A is that the same may happen to a parhelion. This would mean that, during the transition of a normal parhelion into a coronal parhelion, there would be a short intermediate stage where the parhelion is chromospheric, which would result in a temporary appearance of a monochromatic red parhelion.

B. Chromospheric Rainbow

The only pre-1977 description of the appearance of an eclipse rainbow of which we are aware of dates from 1901 and is described by Maunder [18]. The rainbow appeared during the eclipse of 18 May 1901, being one of the deepest of the 20th century, and was observed by several parties in Mauritius. The eclipse rainbow was observed by the party in Quatre Bornes (20° 16′ S, 57° 29′ E), which is 20 km SSW from Maunder's site at Pamplemousses. The total phase of the eclipse occurred with the Sun in NE (azimuth 60.5°) at altitude 18.5°. Mid-eclipse was on 04:03:14 UT, 1 h 31 min after sunrise. The magnitude of the eclipse was 1.026; totality lasted 3 m 40 s.

Although Maunder's account is second-hand (as he himself wrote), it is useful to compare it with the 1977 account. At the time that the 1977 account was written down, the compiler (G. S.) was unaware of the existence of the 1901 paper. Hence, the 1901 and 1977 reports can be treated as mutually independent accounts. Maunder's account reads as follows:

"The observers at Quatre Bornes, watching the eclipse under apparently cloudless sky but in a smart drizzle of rain, saw a rainbow made by the eclipse itself. (. . .) I believe this observation of an eclipse rainbow to be unique. I wish it had been my fortune to see it. (. . .) The three observers all agree that it tapered at the two ends, and one of them was much impressed by bright lines running through it, particularly a bright pink line. Could it be the C line of hydrogen (H-alpha; 656.3 nm) from the large prominence?"

There seems little doubt that the "pink line" has been the same as the thin thread of H-alpha "pink" that was seen in 1977. The fact that the 1977 feature survived for a second or two as the rest of the (photospheric continuum) spectrum faded out coincident with the time of C2 clearly implies its chromospheric origin. In Maunder's account, he does not actually say if the observer's "pink line" was visible during/throughout totality—which could be the case if the large prominence that he saw had been so bright that it outshined the corona. In that case, the "pink line" was not necessarily chromospheric.

However, Maunder's conjecture about the prominence being the cause of the eclipse rainbow seems untenable, for two reasons. First, the brightness of even a monstrous prominence would be too small to outshine the corona, while a perceptible coronal rainbow seems impossible [1]. The argument is as follows. Prominences will have average surface brightness in visible light (typically) about 4× brighter than the surface brightness of the innermost (brightest) part of the corona, regardless of the size of the prominence, and so the total brightness of a prominence will to first order just scale by its surface area.

So, simply put, unless the total surface area of a posited prominence reaches ∼25% of the inner corona, the coronal light will dominate. That ∼25% by area is well beyond what one could reasonably expect, as the largest prominences (other than maybe a once per century event, even then a big stretch) will have a surface area that is much smaller than that of even just the innermost part of the corona. Second, at the 1901 eclipse, there were no large prominences: the Lick Observatory expedition to Sumatra noted during the observation with the 40 ft. telescope the occurrence of only "a number of small prominences, exhibiting considerable detail on the East limb" [19].

The conclusion of G. S.'s and Maunder's reports is that chromospheric rainbows are possible and likely occurred as short-living features during both the 1901 and 1977 eclipses. The two observations contradict the conjecture in the analysis of [1] that the "pink line" in Maunder's report should be attributed to the occurrence of a supernumerary rainbow instead. However, the observation Maunder's "bright lines" (hence more than the "pink" one) that ran through the "eclipse rainbow" remains unexplained by us.

The chromospheric rainbows appeared during the eclipse stage in which the general illumination of the sky by the Sun rapidly decreased. They appeared because, in the very last stage

Fig. 8. This picture, taken just at the end of the 27 s of totality of the eclipse of 4 December 2002, shows that for eclipse magnitudes close to unity, the chromosphere extends over a long arc. As the magnitudes of the 2002 eclipse (1.004) and the 1977 eclipse (1.006) are comparable, the appearance of the Sun at the beginning of totality of the 1977 eclipse probably was similar to this picture. The observing site was at Lindon Station, Fortville Bore, South Australia, 29° 07.9′ S, 140° 53.8′ E. The Sun is very low (1.4° up) in the southwest (azimuth 245.2°). The oblateness of the eclipsed Sun, with the direction toward the zenith up, is due to differential atmospheric refraction across the disk and is best seen when this picture is temporarily turned sideways [22]. (Picture taken by Glenn Schneider.)

before totality, the attenuation in the intensity at the hydrogen H-alpha line is retarded with respect to that of the remainder of the continuum spectrum [20]. At the final stage of partiality, the rainbow has lost its non-H-alpha components, and a red rainbow of smaller width remains. This situation (of different physical causality) is comparable to the transition near sunset of a multispectral rainbow to a red rainbow [7,21]. In the latter case, the primary light source (the setting Sun) is turning red due to atmospheric attenuation that is greatest in the short-wavelength part of its spectrum.

As it seems highly unlikely that the light of a very bright prominence may generate a perceptible rainbow, the chromosphere is the only source capable to create an H-alpha rainbow. A chromospheric rainbow is a short-lived phenomenon occurring only during near-totality. The best chance of it appearing is when the chromosphere extends over a long arc, which is the case when the magnitude of the eclipse is close to 1 (Fig. 8). Such was the case at the 1977 eclipse near sunset.

C. Coronal Versus Chromospheric Rainbows

The two observations of a chromospheric rainbow do not undermine the claim in [1] that "a rainbow during totality seems impossible," as this specifically refers to a coronal rainbow.

However, the 1977 observations during the appearance of the chromospheric rainbow provide observational insight about a potential visibility of coronal rainbows. A direct conclusion from the report is that—at least in 1977—the visibility of a coronal rainbow is considerably lower than that of the chromospheric rainbow, as after C2 no return from a red monochromatic to a multispectral (coronal) rainbow was observed. The fact that the chromospheric rainbow was bright enough to be noticed by an unexpectant observer, while immediately afterwards no trace was seen of a coronal rainbow, suggests that in other cases also the signal-to-background ratio for visual observation of a coronal rainbow is a least a factor 2 lower than for a chromospheric one and is likely to remain below the threshold of human perception.

Table 4. Relative (Unity Normalized to the Total of the Chromospheric 180° Sector) Brightness Measured for the 2002 Eclipse

Decomposed Color Components	Chromospheric 180° Sector	Coronal 90° Sector
Total	100.0%	96.6%
R	72.8%	38.6%
G	14.9%	31.7%
B	12.3%	26.3%

This result—the appearance in 1977 of the chromospheric rainbow and nonappearance of the coronal one—can be understood by the following simple argument. Neglecting the change in sky brightness during the few-seconds-lasting transition to or from totality, the signal-to-background ratio of a rainbow is proportional to its surface brightness (radiance per unit solid angle), and thus proportional to the irradiance of the rainbow-generating drops by the light source. It is also inversely proportional to the scattering-angular width of the radiance distribution of the rainbow. Both visual inspection and photometric measures of Fig. 8 given in Table 4 (as explained in Appendix A.2) suggest that, at least in 2002, the total brightness of the inner corona is comparable to that of a 180° chromospheric arc; simulations (see Appendix A.1) show that the scattering-angle radiance distribution of a multispectral (coronal) rainbow is 5 times wider than the scattering-angle radiance distribution of a monochromatic (chromospheric H-alpha) rainbow. So, the no-show of a coronal rainbow during 1977 should be mainly attributed to the larger than monochromatic scattering-angular width of this multispectral phenomenon rather than to the relative weakness of the light of the corona—a conclusion that is supported by the quantitative analysis presented in the Appendix A.

Although the two unexpectant visual observations of the monochromatic red rainbow illustrate that the signal-to-background ratio of a chromospheric rainbow can be amply above the threshold for visual observation, it seems indeed [1] unlikely that such would ever be the case for a coronal rainbow.

5. CONCLUSION

- A high-resolution time series of photographs taken in 2016 from a high-altitude jet aircraft provided for the first time the opportunity to study the behavior of a subsun before, during, and after the totality of a solar eclipse.
- The pictures taken during the deeply partial phases of the eclipse showed a light spot at the subsun point. The spot can be identified as a subsun.

• Although the subsun-creating conditions most likely persisted during totality, we could not retrieve a coronal subsun from the pictures taken at totality.

• This nondetection does not exclude the possibility of the occurrence of coronal halos. The best candidates are the parhelia, having often a better signal-to-background ratio than a subsun appearing on top of a thick cloud deck.

• A visual observation (by G. S.) during the 1977 solar eclipse is reported of a rainbow that, just before its disappearance during totality, turned from multispectral into monochromatic red.

• Maunder's report of the 1901 solar eclipse describes the same transition of a rainbow. His description of the phenomenon bears large similarities to the 1977 description.

• At the time G. S. saw and recorded the 1977 monochromatic red rainbow, he was unaware of the Maunder 1901 observation, and so any similarities or differences in descriptions were unbiased by expectations.

• These two observations confirm the occurrence, during a few seconds only, of a chromospheric rainbow just before or just after totality.

• A parhelion at the edge of totality is expected to exhibit a similar behavior as a rainbow. Its transition from a multispectral to monochromatic red should be visible by the naked eye. This short-living chromospheric parhelion is still waiting to be observed.

APPENDIX A: SURFACE BRIGHTNESS DETAILS

A.1 Rainbow Widths

In rain showers, the drop size distribution is broad (see, e.g., [23]). Then, the solar disk (0.5° diameter) convolved radiance distributions as a function of scattering angle of monochromic and multispectral rainbows are mutually similar and close to what is expected from geometric optics, in particular near their feet [24]. Therefore, the rainbow width can be regarded to scale with the full width at half-maximum (FWHM) of the scattering-angle distribution of the rainbow. Simulations with Laven's MiePlot program [25] of rainbows show that the FWHM of a solar disk convolved multispectral rainbow is a factor 5.3 larger than the FWHM of a solar disk convolved monochromatic (H-alpha) rainbow.

A.2 Brightness Ratio Solar Chromosphere/Corona

The brightness ratio chromosphere/corona obviously has no data to directly inform on the 1977 event, but to a very rough first order, the geometrically similar 2002 image (Fig. 8) can serve as a (loose) proxy. A 90° wide sector at the upper left part (fourth quadrant) exterior to the solar limb contains only inner coronal light; the third and second quadrants show an extended arc of chromosphere, actually larger than 180° in extent. We scanned the original color picture, decomposed the color image into its R, G, and B components, and measured for each component the total (coronal) brightness in the fourth quadrant and the (chromospheric) brightness in the third and second quadrants (a 180° sector). In doing so, we mask out the Moon interior to the limb and the sky beyond the inner coronal extent to improve the SNR and eliminate the zero-bias. Table 4 shows the relative brightness by color channel, unity normalized in both columns to that of the total chromospheric 180° sector.

The table indicates that based on the 2002 eclipse, the total polychromatic brightness of the inner corona (linearly extrapolating over the full 360°) is about 4 times larger than a 180° long chromospheric arc; assuming for simplicity a biaxially symmetric corona, this factor becomes 2. However, there are several uncertainties in this number: the (monochromatic) chromosphere, in some places, appears to be overexposed. Thus, its R-channel brightness is a lower limit due to image saturation—potentially manifesting itself also in a false signal in the G/B color layers (by halation). Additionally, the 2002 solar elevation angle during totality was very low (1.7°), and instrumental and visual sensitivities are not the same, etc. The bottom line, though, is it seems for the 2002 event the inner coronal and chromospheric total brightness were similar within a factor of ∼2.

Dividing this (rough) estimate of flux ratio between corona and chromosphere by the FWHM ratio (5.3) as obtained above indicates that the signal-to-background ratio for a coronal rainbow could be roughly a factor 2–4 lower than for the 1977 chromospheric rainbow.

Acknowledgment. H. W. van den Brink (KNMI) retrieved and interpolated the ERA5 data. J. Ruitenberg combined the 11 frames that make up Fig. 5. N. Lefaudeux performed an initial analysis of the 2016 eclipse images. The vertical temperature profile at mid-eclipse has been obtained Copernicus Climate Change Service Information [2018]. G. S. thanks Alaska Airlines for their cooperation in the implementation of the flight plan [13], thus enabling the 2016 observations reported here.

Disclosures. The authors declare no conflicts of interest.

REFERENCES

1. G. P. Können and C. Hinz, "Visibility of stars, halos, and rainbows during solar eclipses," Appl. Opt. **47**, H14–H24 (2008).
2. W. E. Sharp, S. M. Silverman, and J. W. F. Lloyd, "Summary of sky brightness measurements during eclipses of the Sun," Appl. Opt. **10**, 1207–1210 (1971).
3. S. M. Silverman and E. G. Mullen, "Sky brightness during eclipses: a review," Appl. Opt. **14**, 2838–2843 (1975).
4. G. E. Shaw, "Sky brightness and polarization during the 1973 African eclipse," Appl. Opt. **14**, 388–394 (1975).
5. W. Tape, *Atmospheric Halos*, Vol. 64 of the Antarctic Research Series (American Geophysical Union, 1994).
6. R. Greenler, *Rainbows, Halos, and Glories* (Cambridge University, 1980).
7. L. Cowley, "Atmospheric Optics website," http://www.atoptics.co.uk/.
8. G. P. Können, "The prodigious halo of the other Huygens," Appl. Opt. **54**, B185–B193 (2015).
9. G. P. Können and R. Schmidt, "Submoon," Weather **68**, 208–209 (2013).
10. J. Küttner and E. Model, "Nebenuntersonne, Unterjupiter und andere Bemerkenswerte Halo-Beobachtungen auf der Zugspitze," Meteorolog. Rundsch. **1**, 218–220 (1948).
11. D. K. Lynch, D. S. B. Dearborn, and J. A. Lock, "Glitter and glints on water," Appl. Opt. **50**, F39–F49 (2011).

12. G. P. Können, *Polarized Light in Nature* (Cambridge University, 1985), Plate 40.
13. G. Schneider, "A unique "serendipitous" total solar eclipse 2016 observation flight opportunity: Intercepting the Moon's shadow from AS flight 870", Personal Document (2015), http://nicmosis.as.arizona.edu:8000/ECLIPSE_WEB/TSE2016/TSE2016_AS870_FLIGHT_OPPORTUNITY_R002_NA.pdf.
14. https://confluence.ecmwf.int/display/CKB/ERA5%3A+data+documentation.
15. X. M. Jubier, Solar Eclipse Maestro program http://xjubier.free.fr/en/site_pages/solar_eclipses/Solar_Eclipse_Maestro_Photography_Software.html.
16. A. Davies and P. Fennessy, *Digital Imaging for Photographers*, 4th ed. (Focal, 2001).
17. http://halostack.readthedocs.io/en/latest/.
18. E. W. Maunder, "The comet and the eclipse," The Observatory **24**, 373–376 (1901).
19. C. D. Perrine, "The Lick Observatory—Crocker Expedition to Observe the Total Solar Eclipse of 1901, May 17–18," Publ. Astron. Soc. Pac. **13**, 187–201 (1901).
20. R. B. Slobins, "Flash spectrum 21/8/2017," https://vimeo.com/231580691.
21. M. Minnaert, *The Nature of Light and Color in the Open Air* (Dover Publications, 1954).
22. A. Meinel and M. Meinel, *Sunsets, Twilights, and Evening Skies* (Cambridge University, 1983), p. 14 and Plate 2-2.
23. J. S. Marshall and W. M. Palmer, "The distribution of raindrops with size," J. Meteorol. **5**, 165–166 (1948).
24. G. P. Können, "Appearance of supernumeraries of the secondary rainbow in rain showers," J. Opt. Soc. Am. **A4**, 810–816 (1987).
25. P. Laven, "MiePlot computer program," https://www.philiplaven.com/mieplot.htm.